Table 5. *Results of the search/match procedure applied to binary oxides* TiO_2 *and* ZrO_2

Binary oxide		Number of hits for 2% tolerance	Examples of derived ternary oxides
TiO_2	Anatase	15	Na_2CoO_2,* K_2HgO_2, Na_2ZnO_2
	Brookite	53	$CuGdO_2$, $TbLiO_2$, $SmCaO_2$
	Rutile	17	Li_2MgO_2, Rb_2BaO_2, K_2SmO_2
	TiO_2(II)	89	$SrPbO_2$, $NaBiO_2$, $NaCeO_2$
ZrO_2	Monoclinic	56	$NaGdO_2$, $NaCfO_2$, $BaSmO_2$
	Tetragonal	59	$PdLiO_2$, $SbLiO_2$, $NaBiO_2$
	Cubic	59	$PdLiO_2$, $SbLiO_2$, $NaBiO_2$

* Co^{2+} ion is in high-spin state.

composition *will* actually adopt the structure derived from the binary oxide. One example in Table 5, $NaBiO_2$, can be derived either from the TiO_2(II) structure, or from the tetragonal/cubic ZrO_2 structure, and the two structures are quite different. Thus the technique is best regarded as as computational tool, to be used in conjunction with experimental structural work. It is also a helpful approach in developing logical connections between observed crystal structures.

References

BURDETT, J. K., HUGHBANKS, T., MILLER, G. J., RICHARDSON, J. W. & SMITH, J. V. (1987). *J. Am. Chem. Soc.* **109**, 3639–3646.

DIEHL, R., BRANDT, G. & SALJE, E. (1978). *Acta Cryst.* B**34**, 1105–1111.

GAVEZZOTTI, A. (1983). *J. Am. Chem. Soc.* **105**, 5220–5225.

GAVEZZOTTI, A. & SIMONETTA, M. (1987). *Organic Solid State Chemistry*, edited by G. R. DESIRAJU, pp. 391–432. Amsterdam: Elsevier.

GREY, I. E., LI, C., MADSEN, I. C. & BRAUNSHAUSEN, G. (1988). *Mater. Res. Bull.* **23**, 743–753.

HOWARD, C. J., HILL, R. J. & REICHERT, B. E. (1988). *Acta Cryst.* B**44**, 116–120.

KEHL, W. L., HAY, R. G. & WAHL, D. (1952). *J. Appl. Phys.* **23**, 212–215.

LOOPSTRA, B. O. & RIETVELD, H. M. (1969). *Acta Cryst.* B**25**, 1420–1421.

MEAGHER, E. P. & LAGER, G. A. (1979). *Can. Mineral.* **17**, 77–85.

MORIKAWA, H., SHIMIZUGAWA, Y., MARUMO, F., HARASAWA, T., IKAWA, H., TOHJI, K. & UDAGAWA, Y. (1988). *J. Ceram. Soc. Jpn Int. Ed.* **96**, 251–256.

RAMDAS, S., THOMAS, J. M., BETTERIDGE, P. W., CHEETHAM, A. K. & DAVIES, E. K. (1984). *Angew. Chem. Int. Ed. Engl.* **23**, 671–679.

SALJE, E. (1977). *Acta Cryst.* B**33**, 574–577.

SHANNON, R. D. (1976). *Acta Cryst.* A**32**, 751–767.

TEUFER, G. (1962). *Acta Cryst.* **15**, 1187.

THOMAS, N. W. (1989). *Acta Cryst.* B**45**, 337–344.

THOMAS, N. W. (1990). Unpublished work.

THOMAS, N. W. (1991). *Acta Cryst.* B**47**, 180–191.

THOMAS, N. W., RAMDAS, S. & THOMAS, J. M. (1985). *Proc. R. Soc. London Ser. A*, **400**, 219–227.

THOMAS, N. W. & THOMAS, J. M. (1986). *Mol. Cryst. Liq. Cryst.* **134**, 155–168.

WYCKOFF, R. (1964). *Crystal Structures*, Vol. 1, p. 243. London: Wiley.

Acta Cryst. (1991). B**47**, 597–608

A New Parametrization for Investigating Relationships Between Chemical Composition and Crystal Structure in Layered ABO_3 Ceramics

BY NOEL W. THOMAS

School of Materials, The University of Leeds, Leeds LS2 9JT, England

(*Received* 1 *October* 1990; *accepted* 25 *February* 1991)

Abstract

The relationship between the layer and framework pictures of layered ABO_3 ceramics is examined, and expressed quantitatively. This permits a calculation of the volumes of cationic coordination polyhedra in terms of AO_3 layer separations and distances between oxygen ions within the layers. Thus the observed stacking sequences (combinations of cubic- and hexagonal-type stacking) can be quantitatively related to the sizes of the cations, and hence chemical composition. Several ABO_3 systems are examined, with Ba^{2+} and Sr^{2+} as A ions. In the (Ba,Sr)RuO_3 system, the occurrence of 9L, 4L and perovskite phases is rationalized in terms of $\langle V_A\rangle/\langle V_B\rangle$ polyhedral volume ratios, and the solubility of different B ions in the 9L $BaRuO_3$ structure is discussed. Considerations of ionic size are generally adequate to understand the structures obtained, except in compounds with the hexagonal barium titanate structure, where metal–metal bonding occurs. The influence of temperature and pressure on stacking sequence is considered, by examining $BaMnO_{3-x}$ and $Ba_{1-y}Sr_yMnO_{3-x}$ compositions. A rationalization in terms of $\langle V_A\rangle/\langle V_B\rangle$ ratios is again found to be appropriate. Whereas the layer picture breaks down

0108-7681/91/050597-12$03.00

in some ABO_3 systems, the framework picture, with its quantitative expression in terms of cationic polyhedral volumes, is of general validity.

Introduction

The structures of many metal oxides of composition ABO_3, where A and B are cations of different size, can be understood in terms of both a framework and a layer picture (Katz & Ward, 1964). In the former, the structures are described as cation coordination polyhedra, which share polyhedral elements, *i.e.* corners, edges and faces. However in the latter, they are described as close-packed layers of composition AO_3, with the B ions occupying octahedral sites between the layers. In general terms, the layer picture requires that the A ions are comparable in size to the oxygen ions, and that the B ions are smaller than the A ions. Thus it is oxides of barium or strontium (A ions), together with transition-metal B ions, that tend to form layered structures. Each picture has advantages not shared by the other: the framework concept emphasizes considerations of cationic size and coordination, whereas the layer picture permits a more global view of a given structure. It is more versatile, for example, in dealing with variations in stacking sequences and the occurrence of polytypism within a given system.

The quantitative relationship between the layer and the framework pictures is developed in this paper. The methodology is applied to ABO_3 systems exhibiting different combinations of hexagonal (h) and cubic (c) stacking, in order to investigate the influence of chemical composition upon stacking sequence. Once the composition of a given ABO_3 system is changed, by substitution with ions of radii different from those of A and B, the primary structural effects can be monitored directly in terms of the modified volumes of the cationic coordination polyhedra (framework picture). Moreover, through the link between the two pictures which is developed here, the observed variation in the stacking sequences of close-packed structures may also be quantitatively related to the chemical composition, by taking the sizes of the cations into account. The same applies to inter-layer spacings and to oxygen-ion separations within the layers (*i.e.* deviations from the ideal of close packing).

Since the parametrization is dependent solely on experimentally determined structural data, it provides a means of investigating experimentally the influence of chemical composition on the stacking sequences of layered compounds, together with associated phenomena such as polytypism and stacking faults. So far, models of polytypism have tended to interpret the phenomenon as an interplay between short- and long-range forces (see, for example, Uppal, Ramasesha & Rao, 1980), although the physical origin of these has not been fully articulated. Use of an approach like the one developed here would allow short-range packing considerations to be accommodated in detail in a future model of polytypism, perhaps leading ultimately to the *chemical control* of stacking sequences. This desirable aim has already been identified by Rao & Thomas (1985).

Structural features of layered ABO_3 systems

The structure of an idealized close-packed AO_3 layer is shown in Fig. 1(*a*). It is composed of oxygen ions located at the vertices of two sets of triangles, $T1$ and $T2$, with A ions occupying the positions indicated by asterisks. The layer has hexagonal axes, so that $T1$ and $T2$ are equilateral triangles. The oxygen–oxygen separation, L, is equal to one half of the unit-cell constant, a. In practice, this oxygen-ion separation is not always equal to L, but rather has two values, $L + \Delta L$ and $L - \Delta L$, such that the *sum* of the two

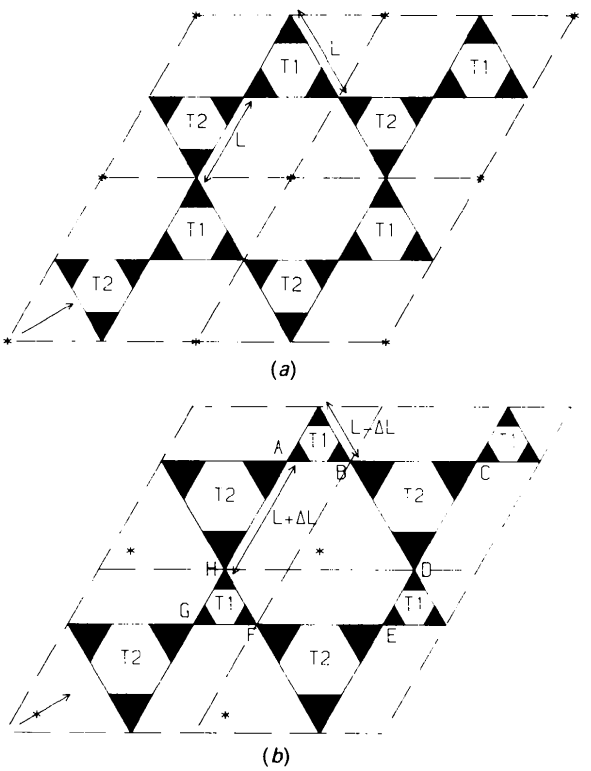

Fig. 1. (*a*) The structure of an idealized close-packed AO_3 layer. Oxygen ions are located at the vertices of equilateral triangles $T1$ and $T2$, which are of equal area; A ions are located at sites denoted by asterisks. Triangles $T1$ and $T2$ are of side L, where L is equal to one half of the unit-cell constant a, referred to hexagonal axes. (*b*) The structure of a generalized AO_3 layer, in which $T1$ and $T2$ triangles maintain their equilateral geometry, but are no longer equal in area: $T1$ is of side $L - \Delta L$, with $T2$ of side $L + \Delta L$.

separations is still equal to the unit-cell constant, a. Thus a more generalized AO_3 layer has the form shown in Fig. 1(b), where there is now in difference in size of the triangular areas $T1$ and $T2$. The transition from the Fig. 1(a) to the Fig. 1(b) structure is effected merely by displacing three rows of oxygen ions, with the equilateral geometry of triangles $T1$ and $T2$ maintained.

The consequences of this structural modification may be appreciated when a second AO_3 layer is added, above and parallel to the first one. The maintenance of 'close packing' dictates that this second layer may be placed in one of two positions with respect to the first. Thus if the first layer is denoted as an A layer, the second layer may be either a B or a C layer, corresponding to the notation commonly used to describe the structures of close-packed metals (h.c.p. and c.c.p.). However, in order to minimize the occurrence of confusing notation, the letters X, Y and Z will henceforth be used to denote A, B and C layers, respectively. The arrows in the bottom left-hand corners of Figs. 1(a,b) denote the direction of the translation in proceeding from an X layer to the Y layer above it, and Figs. 2(a–f) show how three-dimensional structures may be built up from AO_3 layers.

All the diagrams in Fig. 2 are projections along the z axis (stacking axis). Fig. 2(a) is essentially a miniaturized version of Fig. 1(a), to which a second (Y) layer is added in Fig. 2(b). The relative ($X \rightarrow Y$) translation is ($-a/3$, $a/3$, d), where d is the interplanar spacing. Notice how four star-like motifs are obtained, corresponding to regular oxygen-ion octahedra. It is inside these octahedra that the B ions are to be found. If, however, the same relative ($X \rightarrow Y$) translation is applied to the irregular close-packed layer (Figs. 1b and 2d), the oxygen-ion octahedra formed in Fig. 2(e) are no longer regular, owing to the different areas of triangles $T1$ and $T2$. An analysis of the known crystal structures of these compounds shows that the stacking structure depicted in Fig. 2(e) is very rarely found. Instead, an additional operation is carried out prior to the $X \rightarrow Y$ translation. This corresponds to an inversion, whereby a $T1$ triangle is converted into a $T2$ triangle and *vice versa*. The subsequent $X \rightarrow Y$ translation, ($-a/3$, $a/3$, d), generates the structure shown in Fig. 2(f), where regular oxygen-ion octahedra (star shapes) are found again. This structure is commonly found, and in systems with identical X and Y layers (*i.e.* L and ΔL the same for both), the centres of these octahedra have point symmetry $\bar{3}m$.

As with close-packed metals, a further structural feature concerns the location of a *third* close-packed layer: this may either lie directly above the first layer (stacking sequence XYX), or it may be translated relative to the second layer by ($-a/3$, $a/3$, d), to form the sequence XYZ. An XYX sequence may be imagined in Figs. 2(b) and 2(f), since a third layer would be indistinguishable from the first, in projection. An XYZ sequence is shown in Fig. 2(c), for regular close-packed layers. Notice how the octahedra share all their corners with one other. An XYZ sequence is also possible for irregular close-packed layers (not illustrated), although a $T1/T2$ inversion operation is again required, before the second ($-a/3$, $a/3$, d) translation.

The significance of the transition from regular to irregular close-packed layers is best appreciated by comparing Figs. 2(b) and 2(f). Notice how the octahera are much smaller in Fig. 2(f). This implies that the presence of relatively smaller B ions will promote irregular close-packed layers. It also follows that significantly irregular close-packed layers will be associated with $XYXY$, rather than $XYZXYZ$ stacking. Since the latter stacking sequence requires

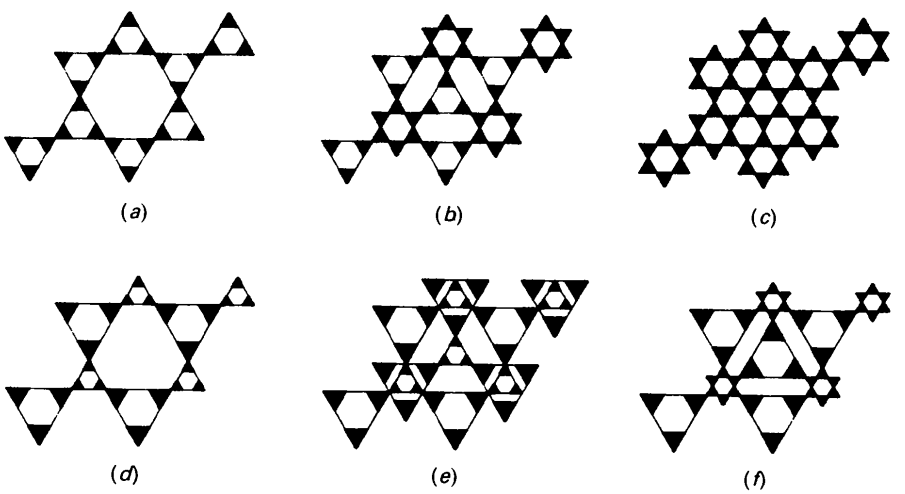

Fig. 2. Possible stacking sequences in ABO_3 structures, viewed in projection perpendicular to the stacking axis. (a) A regular close-packed AO_3 layer, 'X', as in Fig. 1(a). (b) Two regular layers, the second above the first, in an 'XY' sequence. (c) Three regular layers in an 'XYZ' sequence. (d) An irregular AO_3 layer, 'X', as in Fig. 1(b). (e) Two irregular layers, the second related to the first by a simple translation, in an 'XY' sequence. (f) Two irregular layers, also in an 'XY' sequence, but with the second layer generated from the first by a $T1 \leftrightarrow T2$ inversion, followed by a translation.

corner-sharing octahedra, any structure with irregular close-packed layers will necessarily have two sets of oxygen-ion octahedra, of different size. This is unfavourable in systems with only one kind of *B* ion, since a particular ion tends to be associated with a single appropriate octahedral volume in any given structure. This contrasts with an *XYXY* sequence, where only one set of oxygen-ion octahedra is formed, each octahedron sharing two faces with other octahedra to form columns. This columnar structure permits *independent* variation of BO_6 octahedral volumes, to accommodate *B* ions of different sizes.

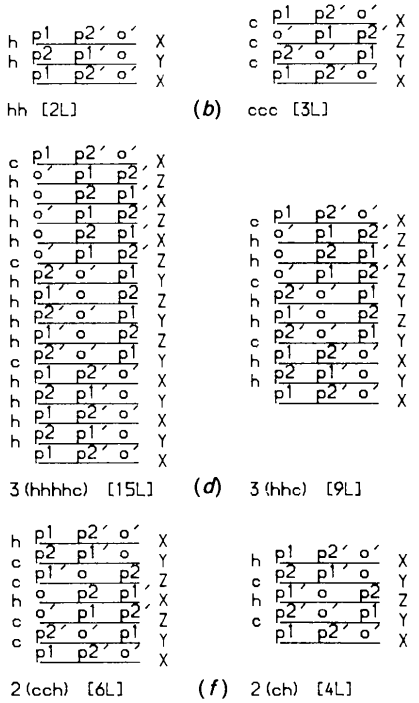

Fig. 3. The inter-relationship between the framework and layer pictures, depicted graphically for six different stacking sequences. The diagrams also show the heights of the columns of face-sharing BO_6 octahedra.

This structural feature is best appreciated by considering different stacking sequences, as viewed along an axis of type ⟨110⟩, as shown in Figs. 3(*a–h*). In these diagrams, each close-packed layer is denoted by a horizontal line, which is ascribed two labels, either *c* or *h* (see left-hand side) and one of *X*, *Y* or *Z* (see right-hand side). A layer is labelled '*c*' if it is coordinated by two dissimilar layers, and '*h*' if coordinated by two similar layers. For example, a *Y* layer would be '*c*' if coordinated by one *Z* and one *X* layer, and '*h*' if coordinated by two *X* layers. The symbols *p*1, *p*2, *p*1′, *p*2′, *o* and *o*′ denote elements of cation coordination polyhedra, as shown in Fig. 4. A further label, 2*L*, 3*L*, 15*L*, *etc.* is given to the structures, denoting the number of layers in the unit cell. In all these structures, the polyhedra share faces in such a manner as to fill space.

Each of the diagrams in Fig. 3 should be read from the bottom upwards. Thus in each case, a *Y* layer follows the bottom *X* layer, with polyhedral elements *p*1, *p*2′ and *o*′ lying between these two layers. To visualize this, consider a unit cell *ACEG*, as in Fig. 1(*b*). Along the view direction [110], the cell diagonal *CG* passes through three polygons, the triangle *T*2 (*BCD*), an irregular hexagon *ABDEFH* and the *T*1 triangle *FGH*. This close-packed layer may be regarded as the bottom (*X*) line in each of Figs. 3(*a–f*). When the *Y* layer is added, as in Fig. 2(*f*), a hexagon is laid above the *T*2 triangle, forming the polyhedron *p*1; a *T*2 triangle is laid above hexagon *ABDEFH*, forming polyhedron *p*2′; and a second *T*1 triangle is laid above *T*1 triangle *FGH*, forming polyhedron *o*′ (see Fig. 4). Both *p* and *o* polyhedra contain eight sides, the *o* being regular octahedra, and the *p* polyhedra containing one hexagonal and seven triangular sides. A *p* polyhedron is numbered 1 if its hexagonal side is uppermost, and 2 if the hexagonal side is at its base. The presence of a prime in the notation for *p* polyhedra denotes that the upper or lower triangular side is pointing into the plane of the paper in Fig. 4, or equivalently, upwards in Figs. 1 and 2. The converse holds for unprimed *p*

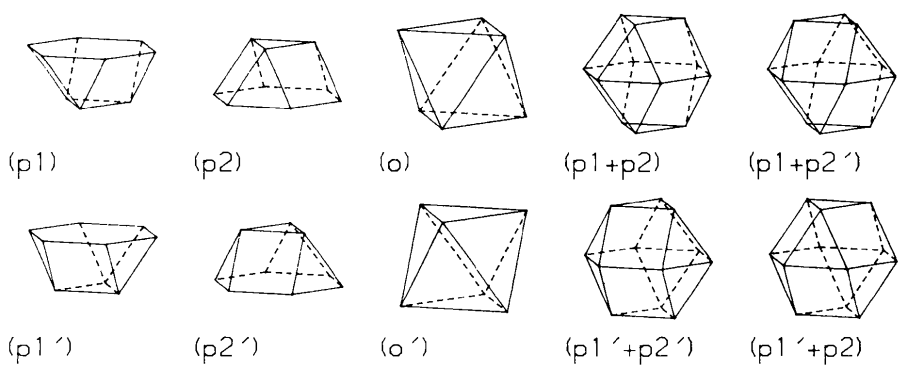

Fig. 4. Definition of polyhedral elements *p*1, *p*1′, *p*2, *p*2′, *o* and *o*′, with the four composite AO_{12} polyhedra (*p*1 + *p*2), (*p*1 + *p*2′), (*p*1′ + *p*2′) and (*p*1′ + *p*2).

polyhedra. Similarly, for *o* octahedra, the presence of a prime indicates that the *lower* triangular side is pointing into the plane of the paper in Fig. 4.

Just as close-packed layer designations *c* and *h* may be decoded directly into stacking sequences in terms of *X*, *Y* and *Z*, there exist simple combination rules for *p* and *o* polyhedra which share faces at *c* and *h* layers. At a *c* layer, the following sequences of polyhedra can occur, proceeding parallel to the *z* axis: *p*1 followed by *p*2′; *p*2 followed by *o*; *p*1′ followed by *p*2; *p*2′ followed by *o*′; *o* followed by *p*1′; *o*′ followed by *p*1. And at an *h* layer, the following combinations are permitted: *p*1 followed by *p*2; *p*2 followed by *p*1; *p*1′ followed by *p*2′; *p*2′ followed by *p*1′; *o* followed by *o*′; *o*′ followed by *o*.

It is seen that all the diagrams in Fig. 3 are constructed in accordance with these combination rules. A further point is that *p* polyhedra are *not* complete *A*-ion coordination polyhedra. To form these, a *p*1 or *p*1′ polyhedron is combined with either a *p*2 or a *p*2′ polyhedron, as shown in the four diagrams to the right-hand side of Fig. 4. So *A*-ion coordination polyhedra span *two* layer spacings, in contrast to *B*-ion octahedra, which span only one. Note that (*p*1 + *p*2) and (*p*1′ + *p*2′) AO_{12} polyhedra have an *h* layer at their centre, whereas (*p*1 + *p*2′) and (*p*1′ + *p*2) have a *c* layer at their centre. Furthermore, the latter two polyhedra have a special name, the cuboctahedron.

Fig. 3 also brings out the well-known structural feature, that *h* layers give rise to face-sharing octahedra, whereas *c* layers give rise to corner-sharing octahedra. Fig. 3(*a*) represents a stacking sequence consisting only of *h* layers (as found, for example in $BaNiO_3$ (Krischner, Torkar & Kolbesen, 1971). Note how the structure consists of infinite columns of face-sharing octahedra (sequence *o*,*o*′,*o*,*o*′,...), together with separate columns of (*p*1 + *p*2) and (*p*1′ + *p*2′) AO_{12} polyhedra. This contrasts with the structure depicted in Fig. 3(*b*), which consists only of *c* layers. This corresponds to the *perovskite* structure, consisting merely of *o*′ BO_6 octahedra and (*p*1 + *p*2′) AO_{12} cuboctahedra. One example of such a structure is given by the complex oxide $Ba(Zn_{1/3}Ta_{2/3})O_3$ (Jacobson, Collins & Fender, 1976).

The remaining diagrams in Fig. 3 correspond to mixtures of *c* and *h* layers, as are frequently encountered. Note how the function of the *c* layers is to break up the columns of face-sharing octahedra. The 5(*hhhhc*) sequence, as found in the $BaMnO_3$ 15*L* structure (Negas & Roth, 1971), consists of columns of five face-sharing octahedra. This contrasts with the 3(*hhc*), 2(*cch*) and 2(*ch*) stacking sequences, which consist of columns of three, two and two face-sharing octahedra, respectively. $BaRuO_3$ (Donohue, Katz & Ward, 1965), hexagonal barium titanate (Burbank & Evans, 1948) and $(Ba,Sr)MnO_3$ (Jacobson & Horrox, 1976) are compounds which exhibit these respective structural types.

The occurrence of face-sharing BO_6 octahedra was originally ascribed to highly specific metal–metal *B*–*B* interactions, which are possible in this type of stacking (Donohue, Katz & Ward, 1966*a*). Whilst this is sometimes an important factor in the stabilization of a phase with face-sharing octahedra, it should be noted that the occurrence of face sharing between like polyhedra is a direct violation of Pauling's Third and Fourth Rules (Pauling, 1960; Thomas, 1991): the ionic model of metal oxides regards metal–metal interactions as repulsive, and therefore unfavourable. It follows from the above arguments that a more general, and less stringent reason for the occurrence of face sharing is connected with the associated columnar structures. In a structure consisting of separate columns of *p* and *o* polyhedra, the *sizes* of the AO_{12} and BO_6 octahedra can be varied independently, thereby accommodating a wider range of cation sizes. By comparison, a structure consisting merely of corner-sharing octahedra [as in the perovskite structure (Fig. 3*b*)] is unable to accommodate such a range of *A* and *B* cations, since there are no longer separate columns of *p* and *o* polyhedra.

According to Pauling's rules for ionic oxides, the occurrence of face sharing between octahedra is less favourable than corner sharing. Thus in systems without specific metal–metal bonding, there will be a tendency to limit the extent of face sharing. This gives a possible basis for understanding the variation in column lengths between the different structures in Fig. 3. One might also anticipate that the occurrence of face-sharing octahedra will be less widespread in complex metal oxides, consisting of more than one type of *A* and/or *B* ion, $A',A''(B',B'')O_3$, since the presence of different sizes of *A* and/or *B* ions will allow corner-sharing octahedra between more irregular (*i.e.* greater ΔL) close-packed layers. In general, therefore, the greater the number of different cations present, the more likely it is that a means will be found to adopt a perovskite-like structure, based on corner-sharing octahedra.

Development of a quantitative parametrization for these structures

Having introduced several appropriate structural concepts, a quantitative parametrization is now developed, whereby the above criteria can be investigated in experimentally determined crystal structures. The results obtained permit calculation of the volume of cationic coordination polyhedra as a function of the parameters in the layer picture, which correspond, essentially, to oxygen-ion separations within and between layers. This is valuable both for

the full analysis of structural data and for the comparison of related systems. However, if the sole aim is the calculation of polyhedral volumes, *per se*, it is advisable to use the simpler computational method developed earlier (Thomas, 1989, 1991).

In order to monitor quantitatively the effects of varying chemical composition on the stacking sequences, it is necessary to develop expressions for the volumes of p and o polyhedra in terms of the distances between the oxygen ions that form them. Fig. 5(*a*) shows the three lengths, A, B and C, which, together with the inter-layer spacing, d, are necessary to calculate the volume of a generalized p or p' polyhedron. In the following parametrization, the convention is adopted that the *vertices of the triangle of side C*, which lies either above or below the hexagon of sides A and B, *point towards the midpoint of the sides of length A*. Similarly, Fig. 5(*b*) shows the two lengths, D and E, which, together with the inter-layer spacing d, are needed to calculate the volume of a generalized o or o' octahedron.

Both calculations utilize a general result, which may be inferred from Fig. 5(*c*). This shows a hexagon with two unequal edge lengths, l_1 and l_2, but with all internal angles equal to 120°. The area, A_h, of this hexagon is equal to the sum of the areas of the three parallelograms and that of the central equilateral triangle, *i.e.*

$$A_h = 3^{1/2}/4(l_1^2 + 4l_1l_2 + l_2^2). \quad (1)$$

In order to calculate the volume of the p polyhedron (Fig. 5*a*), the following variation of l_1 and l_2 with height, z, is assumed:

$$l_1 = A(1 - z/d); \quad (2)$$

$$l_2 = B + (C - B)z/d. \quad (3)$$

Thus for the purposes of the calculation, the triangle is regarded as lying a distance d above the hexagon, which is at height $z = 0$. When $z = 0$, $l_1 = A$ and $l_2 = B$, corresponding to the hexagon in Fig. 5(*a*). And when $z = d$, $l_1 = 0$ and $l_2 = C$, corresponding to the triangle in Fig. 5(*a*). For values of z between 0 and d, l_1 and l_2 vary linearly, as defined in equations (2) and (3).

The volume of the p polyhedron is obtained from the integral

$$V_p = \int_0^d A_h(z)\,dz, \quad (4)$$

where $A_h(z)$ is obtained by substitution for l_1 and l_2 in equation (1) from equations (2) and (3). This gives the following result:

$$V_p = (3^{1/2}/12)(A^2 + B^2 + C^2 + 4AB + 2AC + BC). \quad (5)$$

In the case of the o or o' octahedra (Fig. 5*b*), the variation of l_1 and l_2 is as follows:

$$l_1 = D(1 - z/d), \quad (6)$$

$$l_2 = Ez/d. \quad (7)$$

Thus when $z = 0$, the polygon in Fig. 5(*c*) corresponds to a triangle of side D, and when $z = d$, it corresponds to a triangle of side E. At intermediate values of z, the polygon corresponds to a hexagon with varying degrees of irregularity.

Substitution of equations (6) and (7) into (1), followed by integration according to equation (4) yields the following result:

$$V_o = (3^{1/2}d/12)(D + E)^2. \quad (8)$$

Equations (5) and (8) are the only two results required for a *complete* description of the variation in volumes of the p and o polyhedra with the parameters, A, B, C, D, E and d, representing the separations of oxygen ions in these close-packed layered structures. In calculating the volume of an AO_{12} coordination polyhedron, it is necessary to sum the volumes of *two p* polyhedra.

In order to illustrate this point, and to give a fundamental result, the special case of all the close-packed layers being *regular* is now considered, *i.e.* $A = B = C = D = E = L$. Substitution into equations (5) and (8) gives $V_p = 3^{1/2}\,5/6dL^2$ and $V_o = 3^{1/2}/3dL^2$. Thus the ratio of the A- and B-ion polyhedral volumes, V_A/V_B, which is given by $2V_p/V_o$, is exactly equal to 5. So any structure composed of equally spaced regular close-packed layers will have a V_A/V_B ratio equal to 5, irrespective of its stacking sequence. It is also relevant to recall that this result has been

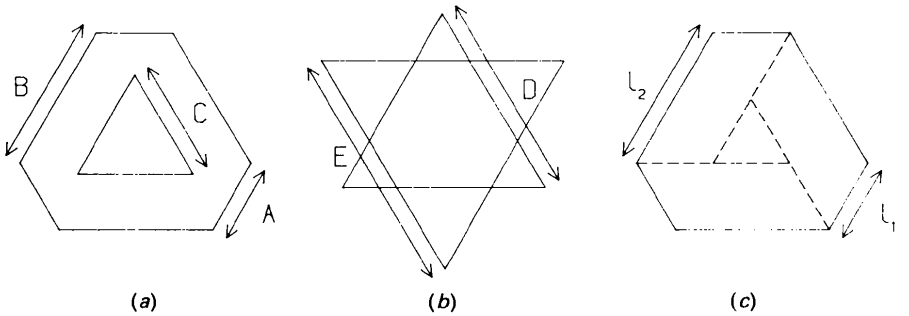

(*a*) (*b*) (*c*)

Fig. 5. (*a*) Definition of parameters A, B and C in equations (2), (3) and (5). (*b*) Definition of parameters D and E in equations (6), (7) and (8). (*c*) Definition of parameters l_1 and l_2 in equations (1), (2), (3), (6) and (7).

Table 1. *An analysis of the* $x = 0$ *and* $x = \frac{1}{6}$ *structures in the* $Ba_{1-x}Sr_xRuO_3$ *system*

	AO_2 layer sequence	Terms in equation (5) (Å)						BO_6 layer sequence	Terms in equation (8) (Å)		
x	xyz	A_y	B_y	C_x	d_{yx}	C_z	d_{yz}	xy	D_x	E_y	d_{xy}
0	*hhc*	2·691	3·059	3·059	2·506	2·875	2·347	*hc*	2·691	2·875	2·347
	hch	2·875	2·875	3·059	2·347	3·059	2·347	*hh*	2·691	2·691	2·506
$\frac{1}{6}$	*chc*	2·782	2·930	2·856	2·372	2·856	2·372	*hc*	2·782	2·856	2·372
	hch	2·856	2·856	2·930	2·372	2·930	2·372				

Table 2. *Polyhedral volumes and deviations from oxygen-ion close packing in the* $Ba_{1-x}Sr_xRuO_3$ *system*

	AO_2 layer sequence			Deviations in A polyhedra (Å)					BO_6 layer sequence			Deviations in B octahedra (Å)			
x	xyz	n_A	V_A (Å)	ΔL_y	ΔL_x	ΔL_z	Δd_{yx}	Δd_{yz}	xy	n_B	V_B (Å)	ΔL_x	ΔL_y	Δd_{xy}	$\langle V_A\rangle/\langle V_B\rangle$
0	*hhc*	6	58·43	0·18	+0·18	0·0	+0·11	−0·05	*hc*	6	10·50	−0·18	0·0	−0·05	5·55
	hch	3	57·82	0·0	+0·18	+0·18	−0·05	−0·05	*hh*	3	10·48	−0·18	−0·18	+0·11	
$\frac{1}{6}$	*chc*	2	55·70	0·07	0·0	0·0	0·0	0·0	*ch*	4	10·88	−0·07	0·0	0·0	5·16
	hch	2	56·58	0·0	+0·07	+0·07	0·0	0·0							

obtained for a particular stacking sequence, *ccc*, in an earlier study (Thomas, 1989). This work used a computational (*i.e.* non-algebraic) method to show that regular perovskites always have a V_A/V_B polyhedral volume ratio of 5.

Application of the parametrization to known crystal structures

The $Ba_{1-x}Sr_xRuO_3$ *system*

Donohue *et al.* (1966*a*) have carried out a study of this system, in which the effect of varying x on the stacking sequence has been monitored. When $x = 0$, a nine-layer (9*L*; Fig. 3*d*) unit cell is obtained, with layer sequence 3(*chh*) (Donohue *et al.*, 1965). As x is increased to $\frac{1}{6}$, a four-layer (4*L*; Fig. 3*f*) unit cell [sequence 2(*ch*)] becomes stabilized. Finally, as x takes on values between approximately 0·5 and 1, a perovskite phase (layer sequence *ccc*; Fig. 3*b*) is formed.

Table 1 gives an analysis of the 9*L* and 4*L* structures. The column headed 'AO_{12} layer sequence, *xyz*' identifies the type of AO_{12} coordination polyhedron, by giving the types of the three close-packed layers forming it. If the middle layer (*i.e.* second symbol, *y*) is of type *c*, the polyhedron is a cuboctahedron [(*p*1 + *p*2′) or (*p*1′ + *p*2)], and if it is of type *h*, the polyhedron is of of type (*p*1 + *p*2) or (*p*1′ + *p*2′). Six parameters, A_y, B_y, C_x, d_{yx}, C_z and d_{yz} are needed for the calculation of the volume of a complete AO_{12} polyhedron, which proceeds in two parts. First, the volume of the lower portion (*i.e.* *p*1 or *p*1′) is calculated, by setting $A = A_y$, $B = B_y$, $C = C_x$, $d = d_{yx}$, and substituting these values into equation (5). Secondly, the volume of the upper portion of the polyhedron is calculated, for which two options exist: (i) $A = A_y$, $B = B_y$; or (ii) $A = B_y$, $B = A_y$. Since the convention is being adopted that the vertices of the triangle of side C point towards the midpoints of the sides of length A, option (i) applies to (*p*1 + *p*2) and (*p*1′ + *p*2′) polyhedra (middle layer *h*), and option (ii) to (*p*1 + *p*2′) and (*p*1′ + *p*2) cuboctahedra (middle layer *c*). Thus the appropriate values of A and B, together with $C = C_z$, $d = d_{yz}$ are substituted into equation (5) to obtain the volume of the upper portion. The net AO_{12} volume is simply the sum of the volumes of the upper and lower portions.

Octahedral volumes are calculated from values of D_x, E_y and d_{xy} by substituting $D = D_x$, $E = E_y$ and $d = d_{xy}$ into equation (8). In this case, the polyhedra are formed from just two close-packed layers. It is also noted from Table 1 that, for this system, A_y and B_y differ only when the y layer is of h character. When it is of c character, $A_y = B_y$. This feature is directly related to the sharing of octahedral *corners* at c layers. In any system with a single B ion, and ideally single BO_6 octahedral volume, the adoption of a regular c layer ensures that both octahedral triangular faces within that layer are of equal area.

Table 2 gives the polyhedral volumes V_A and V_B in the $Ba_{1-x}Sr_xRuO_3$ system, calculated from the parameters in Table 1. An independent check of these volumes has also been made by using a different computer algorithm (Thomas, 1991). Note that n_A,n_B correspond to the numbers of AO_{12} and BO_6 polyhedra of each type in a unit cell. If L is taken to represent the O—O separation in a regular close-packed layer ($L = a/2$, see Fig. 1*a*), an AO_{12} polyhedron has edge lengths ($L + \Delta L_y$) and ($L - \Delta L_y$) in its middle layer, with edge lengths of ($L + \Delta L_x$) and ($L + \Delta L_z$) in its lower and upper layers, respectively. Similarly, a BO_6 octahedron has edge lengths $D_x = L + \Delta L_x$ and $E_y = L + \Delta L_y$. Parameters Δd_{yx}, Δd_{yz} and

Δd_{xy} represent deviations in inter-layer spacing. Thus $\Delta d_{yx} = d_{yx} - c/n$, *etc.*, where c is the length of the c axis, and n is the number of close-packed layers in the unit cell.

It is to be noted that the magnitudes of ΔL_x, ΔL_y and ΔL_z are generally larger for the $x = 0$ compound. The same applies to d values, which are equal to zero in the $x = \frac{1}{6}$ compound. The consequences are directly observed by comparing polyhedral volumes, V_A and V_B, and the volume ratio $\langle V_A\rangle/\langle V_B\rangle$. Values of V_B are similar in both compounds, whereas V_A values fall as x is increased from 0 to $\frac{1}{6}$. This is reflected in $\langle V_A\rangle/\langle V_B\rangle$, which falls from 5·55 when $x = 0$ (A ion = Ba^{2+}) to 5·16 when $x = \frac{1}{6}$ (A ion = $Ba^{2+}_{5/6}$, $Sr^{2+}_{1/6}$). Larger values of ΔL permit the A-ion polyhedral volume to be increased relative to the B-ion volume. Since the Ba^{2+} ion is larger than the Sr^{2+} ion [$r^{XII}(Ba^{2+}) = 1{\cdot}61$; $r^{XII}(Sr^{2+}) = 1{\cdot}44$ Å (Shannon, 1976)], it is to be expected that ΔL will be larger in the $x = 0$ compound.

If the trend of decreasing $\langle V_A\rangle/\langle V_B\rangle$ with increasing x is continued, at a certain critical value of x, a polyhedral volume ratio exactly equal to 5 will be obtained. This is significant, since the system will then be able to pack in a lower-energy perovskite structure, with no face-sharing BO_6 octahedra. An approximate calculation may be made of the value of x at which this is expected to occur: when $x = 0$, $\langle V_A\rangle = 58{\cdot}227$ Å and when $x = \frac{1}{6}$, $\langle V_A\rangle = 56{\cdot}140$ Å^3. Assuming a linear variation, $\langle V_A\rangle/$Å$^3 = 58{\cdot}227 - 12{\cdot}522x$. Taking a mean value of V_B equal to 10·687 Å^3 for both compounds, since the B ion, Ru^{4+}, is invariant, $\langle V_A\rangle/\langle V_B\rangle$ will be equal to 5 when $x = 0{\cdot}38$. So a transition to the perovskite structure is anticipated when $x = 0{\cdot}38$.

This concurs with experimental observations: a perovskite phase begins to be stabilized at approximately $x = \frac{1}{3}$, together with the $4L$ phase. For values of x greater than $\frac{1}{2}$, a single perovskite phase is observed (Donohue *et al.*, 1966*a*). When $x = 1$, an *orthorhombic* perovskite phase is observed (Randall & Ward, 1959). This is consistent with the hypothetical variation of $\langle V_A\rangle$ with x given above: when $x = 1$, $\langle V_A\rangle/\langle V_B\rangle$ is predicted to be 4·27. All orthorhombic perovskites previously investigated have had $\langle V_A\rangle/\langle V_B\rangle \leq 5$ (Thomas, 1989).

$BaRu_{1-x}M_xO_3$ *systems* ($M = Zr^{IV}$, Mn^{IV}, Ni^{II}, Mg^{II})

Donohue, Katz & Ward (1966*b*) have also investigated the phases obtained when the Ru^{IV} ion in $BaRuO_3$ is partly substituted by another metal ion, M, corresponding to Zr^{IV}, Mn^{IV}, Ni^{II} or Mg^{II}. Their observations are summarized here:

(i) No Zr^{IV} may be incorporated in the $9L$ $BaRuO_3$ structure, whereas Ru^{IV} is readly taken up in solid solution in the $BaZrO_3$ structure.

(ii) Mn^{IV} can be substituted completely and randomly in the $9L$ $BaRuO_3$ structure, whereas Ru^{IV} cannot be substituted in the $2L$ lower-temperature form of $BaMnO_3$ (Fig. 3*a*).

(iii) Nickel exists in an oxidation state of +2, rather than +4, at preparative temperatures, so, like Mg^{II}, forms compounds with *pentavalent* ruthenium. The overall composition $Ba\,Ru^{V}_{2x}Ru^{IV}_{1-3x}M_xO_3$ ($M = Ni^{II}$, Mg^{II}) is found as a two-phase combination of $(1-3x)[BaRu^{IV}O_3]$ and $3x[BaRu^{V}_{2/3}M_{1/3}O_3]$. The former compound adopts the $9L$ $BaRuO_3$ structure, and the latter the so-called hexagonal barium titanate structure.

Observations (i) and (ii) reveal a non-reciprocity in substitution patterns, which can be discussed in terms of the present parametrization. It appears that a smaller ion (Mn^{IV}) can be substituted into the $BaRuO_3$ structure, whereas a larger ion (Zr^{IV}) cannot. Similarly Ru^{IV}, which is larger than Mn^{IV}, cannot be substituted in the $2L$ $BaMnO_3$ phase. This selectivity, which is rather surprising, is probably associated with the occurrence of columns of face-sharing octahedra in the $2L$ and $9L$ phases. It appears that arguments based on averaged polyhedal volumes, which are permitted to lie within certain allowed ranges (Thomas, 1989), are not applicable here. A possible justification for this behaviour is that columnar structures are inherently less able to accommodate dopant ions than perovskites. A foreign ion in one octahedral site would necessarily alter the volume of the adjacent octahedral site(s) in the column, in which non-dopant ion(s) would be located. In non-columnar perovskites, however, changes in octahedral volumes can be accommodated by distortions in AO_{12} cuboctahedra, without affecting the volumes of local BO_6 octahedra adversely.

The $9L$ $BaRuO_3$ structure, with its 3(*chh*) stacking sequence, has $\frac{1}{3}$ c-type layers (corner-sharing octahedra) and $\frac{2}{3}$ h-type layers (face-sharing octahedra), so the c layers may permit the substitution of smaller ions, by distortions of adjoining AO_{12} polyhedra. The same argument applied to the $2L$ $BaMnO_3$ structure, with no c layers, would imply very limited solubility of foreign ions in this structure.

Although no full structural determination has been made for the latter composition, it is thought to be isostructural with $BaNi^{IV}O_3$ (Negas & Roth, 1971), for which the structure is known (Krischner *et al.*, 1971). According to their data, $V_A/V_B = 6{\cdot}41$ in this compound, the largest value obtained amongst all the compounds in the present study. This polyhedral ratio is achieved by a large deviation, ΔL, of 0·28 Å in *each* AO_3 layer. Thus the adoption of infinite columns of face-sharing octahedra, as in the $2L$ structure, is directly connected with a large V_A/V_B ratio. Support for this generalization is given from

Table 3. *Polyhedral volumes and deviations from oxygen-ion close packing in compositions with the hexagonal barium titanate structure*: (*A*) $BaTiO_3$ (*Burbank & Evans*, 1948); (*B*) $Ba_3NiSb_2O_9$ (*Koehl & Reinen*, 1977)

	AO_3 layer sequence			Deviations in *A* polyhedra (Å)				BO_6 layer sequence			Deviations in *B* octahedra (Å)			
	xyz	n_A	V_A (Å)	ΔL_x	ΔL_y	ΔL_z	Δd_{yx}	Δd_{yz}	*xy*	n_B	V_B (Å)	ΔL_x	ΔL_y	Δd_{xy}	$\langle V_A\rangle/\langle V_B\rangle$
A	*chc*	2	56·61	0·38	−0·05	−0·05	+0·10	+0·10	*cc*	2	9·82	−0·05	−0·05	−0·21	5·58
	hcc	2	56·54	0·05	+0·38	+0·05	+0·10	−0·21	*ch*	4	10·30	−0·38	+0·05	+0·10	
B	*c′hc″*	2	59·14	0·25	−0·03	−0·12	+0·10	+0·02	*c′c″*	2	10·65	−0·03	−0·12	−0·12	5·35
	hc′c″	2	60·62	0·03	−0·25	−0·12	+0·10	−0·12	*c′h*	2	11·40	+0·03	−0·25	+0·10	
	hc″c′	2	59·14	0·12	+0·25	−0·03	+0·02	−0·12	*c″h*	2	11·37	+0·12	−0·25	+0·02	

an analysis of the 15*L* structure of $BaMnO_3$ (Negas & Roth, 1971), which has columns of five face-sharing octahedra (Fig. 3*c*). The calculated value of $\langle V_A\rangle/\langle V_B\rangle$ of 6·18, also large, suggests that, as the length of the columns increases, there is a concomitant increase in polyhedral volume ratio.

The solubility of Ru^{IV} in $BaZrO_3$ is to be expected, since the barium ion polyhedral volume, at 61·4 Å^3, is very large in this perovskite structure (Thomas, 1989). Incorporation of the smaller Ru^{IV} ion will permit a favourable reduction of V_{Ba}, since $\langle V_B\rangle$ will fall, and $\langle V_A\rangle = 5\langle V_B\rangle$ in perovskites.

With respect to the third observation, it is entirely logical that a two-phase mixture should result, as the substituting ions give rise to changes in oxidation state of the ruthenium ions. It is perhaps less obvious, however, why the compound $BaRu^{V}_{2/3}M_{1/3}O_3$ adopts the hexagonal barium titanate structure, instead of packing as a complex perovskite. Compositions giving rise to the former structure are reviewed in the following section.

The hexagonal barium titanate structure

The first crystallographic determination of the 'hexagonal barium titanate structure' was made by Burbank & Evans (1948), who identified a 2(*cch*) [6*L*] stacking sequence (Fig. 2*e*). Dickinson, Katz & Ward (1961) subsequently suggested that the composition of the crystal used by Burbank & Evans did not correspond exactly to $BaTiO_3$, but rather contained platinum impurities, picked up from a crucible. Following a systematic study of compositions of formula $Ba(M_{1/3}Ti_{2/3})O_3$ (M = Ti^{III}, V, Cr, Mn, Fe, Co, Ru, Rh, Ir, Pt), they proposed that the stabilization of this phase depends upon metal–metal bonding between pairs of *B* cations in the face-sharing octahedra. In order for this to occur, at least one of these cations must have a partially filled *d* shell.

Although accurate structural determinations of compositions adopting this structure are scarce, two such structures are analysed in Table 3. The notation in the table is identical to that in Table 2, except for a detail in the second structure, $Ba_3NiSb_2O_9$ (labelled '*B*'), which contains two different types of *c* layers, denoted by *c′* and *c″*. In this structure, Ni^{II} ions occupy *c″h* octahedral sites, with Sb^{V} ions occupying *c′c″* and *c′h* sites. The largest value of ΔL, 0·25, occurs in the *h* layer, with smaller values of 0·03 and 0·12 occurring in the *c′* and *c″* layers, respectively.

A number of other structural investigations have been made on compositions packing in the hexagonal barium titanate structure, but idealized regular oxygen positional parameters have been adopted, without refinement. This is chiefly due to the relatively small X-ray scattering factor of oxygen, and the associated difficulty in determining accurate oxygen parameters from X-ray powder diffraction studies. These compositions include various complex oxides of barium, *e.g.* Ba_2InRuO_6 (Schaller & Kemmler-Sack, 1981), $Ba_3SmRu_2O_9$ (Thumm, Treiber & Kemmler-Sack, 1981) and $Ba_3NiIr_2O_9$ (Treiber, Kemmler-Sack & Ehmann, 1982). Unfortunately, regular oxygen positional parameters preclude a meaningful polyhedral analysis, since V_A/V_B is always equal to 5, and all values of ΔL and Δd are equal to zero.

However, the limited data in Table 3 support the notion that metal–metal bonding does play a role in stabilizing this structure. In the absence of this bonding, Pauling's rules would favour the adoption of a perovskite structure. This is known to be an option for $BaTiO_3$, and the second composition, $Ba_3NiSb_2O_9$ could also pack as a perovskite: taking a mean *B*-ion polyhedral volume, $\langle V_B\rangle$ of 11·14 Å^3, a perovskite $\langle V_A\rangle/\langle V_B\rangle$ ratio of 5 would give a value of 55·70 Å^3 for $\langle V_{Ba}\rangle$, which lies within the known polyhedral volume range of the Ba^{2+} ion (Thomas, 1989).

The influence of temperature and pressure on stacking sequence

Comprehensive studies of the effects of temperature on stacking sequences have been made for the $BaMnO_{3-x}$ (Negas & Roth, 1971) and $Ba_{1-y}Sr_yMnO_{3-x}$ (Negas, 1973) systems. In the first of these, the following series of structures is observed, at temperatures above 1273 K.

$$2L \xrightarrow{1423\ K} 15L \xrightarrow{1573\ K} 8L \xrightarrow{1623\ K} 6L \xrightarrow{1748\ K} 10L \xrightarrow{1823\ K} 4L.$$

Table 4. *A quantitative analysis of the breakdown of the layer picture in tetragonal and orthorhombic perovskites*

System		Conventional unit-cell constants (Å, °)			Constants of transformed unit cell (Å, °)			σ_O (Å)	V_A/V_B	Ref.*
		a	b	c	a	b	c			
		α	β	γ	α	β	γ			
$BaTiO_3$	(cubic)	3·996	3·996	3·996	5·651	5·651	6·921	0·0	5·00	(1)
		90·0	90·0	90·0	90·0	90·0	120·0			
$BaTiO_3$	(rhombohedral)	4·004	4·004	4·004	5·656	5·656	6·951	0·0	5·00	(2)
		90·0	90·0	90·0	90·0	90·0	120·0			
$BaTiO_3$	(tetragonal)	3·995	3·995	4·034	5·650	5·677	6·942	$1·42 \times 10^{-4}$	5·00	(3)
		90·0	90·0	90·0	90·46	90·0	119·84			
$BaTiO_3$	(orthogonal)	3·990	5·669	5·682	5·659	5·669	6·943	$9·17 \times 10^{-3}$	5·00	(4)
		90·0	90·0	90·0	90·0	90·32	120·06			
$PbTiO_3$	(tetragonal)	3·905	3·905	4·156	5·523	5·703	6·912	0·070	5·00	(5)
	298 K	90·0	90·0	90·0	87·06	90·0	118·96			
$CaTiO_3$	(orthogonal)	5·380	5·442	7·640	7·640	5·407	7·652	0·170	4·62 (6)	
		90·0	90·0	90·0	89·54	90·0	134·95			

* References: (1) Edwards *et al.* (1951); (2) Schildkamp & Fisher (1981); (3) Harada *et al.* (1970); (4) Shirane *et al.* (1957); (5) Glazer *et al.* (1978); (6) Sasaku *et al.* (1987).

Note that the 6*L* phase does *not* correspond to the hexagonal barium titanate structure.

As the temperature is increased, $BaMnO_{3-x}$ becomes progressively more reduced (*i.e.* x increases), with the accompanying reduction from Mn^{IV} to Mn^{III}. Since the radius of the Mn^{III} ion is larger than that of Mn^{IV}, Negas & Roth argue that the larger Mn^{III} ion breaks up the columns formed by *h* layers, with a corresponding increase in *c*-type packing. (Note that a similar argument was invoked above, to rationalize why Zr^{IV} is not soluble in $BaRuO_3$). X-ray diffraction studies support the transition to a greater proportion of *c*-type layers as x is increased. The proportions of *c*-type packing are as follows: 2*L* 0; 15*L* 20; 8*L* 25; 6*L* 33; 10*L* 40; 4*L* 50%. A similar sequence of phases would be anticipated for an increasing hydrostatic pressure, since short metal–metal interactions, which are *repulsive* according to the ionic model, could be reduced by adopting a greater proportion of *c*-type stacking.

In the subsequent study of the $Ba_{1-y}Sr_yMnO_{3-x}$ system, Negas was able to monitor the dependence of stacking sequence upon both x and y. It is interesting to note that his interpretation of the results rests upon a discussion of the effective volumes of the *A* and *B* cations. As y increases, $\langle V_A \rangle$ falls, since the Sr^{2+} ion is smaller than the Ba^{2+} ion. This, and the result that $\langle V_B \rangle$ increases as x rises, may be summarized by stating that $\langle V_A \rangle / \langle V_B \rangle$ decreases with increasing x and y. A consequence of increasing y is that the 4*L* phase may be stabilized at temperatures below 1823 K, the temperature required in $BaMnO_{3-x}$

Thus a steady decrease in $\langle V_A \rangle / \langle V_B \rangle$ is expected in proceeding along the above sequence from the 2*L* to the 4*L* phase of $BaMnO_{3-x}$. As with compositions adopting the hexagonal barium titanate structure, accurate structural data are not available for all phases. However, there is strong evidence to support this trend. $\langle V_A \rangle / \langle V_B \rangle \simeq 6·41$ for the 2*L* phase (see above) and is equal to 6·18 in the 15*L* phase. Independent studies of 4*L* structures of composition $(Ba_{0·1}Sr_{0·9})MnO_3$ (Jacobson & Horrox, 1976) and $SrMnO_3$ (Battle, Gibb & Jones, 1988) give smaller $\langle V_A \rangle / \langle V_B \rangle$ ratios of 5·51 and 5·54, respectively, again consistent with the trend. Note that, on heating $SrMnO_{3-x}$ ($x > 0·25$) to temperatures above 1673 K, a transformation to a perovskite phase occurs (Negas & Roth, 1970). In this instance, $\langle V_A \rangle / \langle V_B \rangle$ is falling further to the value of 5, by reduction of Mn^{IV} to Mn^{III}.

It appears, therefore, that the influence of temperature and pressure on stacking sequence can also be accommodated in the present parametrization.

The breakdown of the layer picture in tetragonal and orthorhombic perovskites

For ABO_3 compounds of hexagonal, rhombohedral and cubic symmetry, the layer picture is capable of accommodating all structural features. However, for perovskites of tetragonal, orthorhombic and conceivably lower symmetry, this picture breaks down. An overall assessment of this may be made by transforming the conventional unit-cell axes for each structure to a new set of axes (x', y', z'), in which the AO_3 layers lie perpendicular to the z' axis. The lengths of the x' and y' unit-cell axes are calculated by identifying the *A*-ion repeat motif in the (x', y') plane. Table 4 shows the results of this procedure.

It is seen that the transformed unit-cell axes correspond to hexagonal axes in cubic and rhombohedral $BaTiO_3$, with the layer picture appli-

cable to both structures. In the cubic polymorph, $\Delta L = 0$, whereas $\Delta L = 0{\cdot}040$ Å in the layers of the rhombohedral phase. Despite this, a V_A/V_B ratio of 5 is maintained through the absence of a $T1 \leftrightarrow T2$ inversion between successive layers, as shown schematically in Fig. 2(*e*). Note, however, that the transformed axes are not hexagonal for the tetragonal and orthorhombic structures. Thus the simple geometry of the layer picture, based on equilateral triangles, is no longer applicable. The parameter σ_O represents the average r.m.s. deviation of the oxygen ions from the (x', y') plane to which they would belong in the idealized layer picture. This is equal to zero in cubic and rhombohedral barium titanate, increasing to 0·170 Å in orthorhombic $CaTiO_3$. In general terms, the greater the orthorhombic or tetragonal distortion (associated either with ferroelectricity or with octahedral tilting), the larger the value of σ_O which is obtained. Note that this analysis neglects the significant deviations from close packing to be found *within* the layers: these are complex, and cannot be described by the two parameters L and ΔL used above for truly layered structures.

In comparison with the layer picture, the framework approach is applicable to all ABO_3 structures, regardless of their symmetry. Coupled with the evaluation of polyhedral volumes, V_A and V_B, and their ratios, it provides a versatile quantitative description of these, and other ceramic systems. It is also a refinement of the Goldschmidt criterion, which states that the factor $t = (R_A + R_B)/2^{1/2}(R_B + R_O)$ must be close to 1 for the perovskite phase to be stabilized. Application of this criterion to some of the compounds studied here, with the radii of Shannon (1976), yields the following values: $BaNiO_3$ 1·132; $BaMnO_3$ 1·102; $BaRuO_3$ 1·064; $BaTiO_3$ 1·062; $SrTiO_3$ 1·002; $CaTiO_3$ 0·966. Thus t values greater than 1 are more likely to be associated with structures containing face-sharing BO_6 octahedra, as in $BaNiO_3$, $BaMnO_3$ and $BaRuO_3$. As discussed previously (Thomas, 1989), there is a corresponding variation in V_A/V_B parallel to that of t. For example, V_A/V_B is equal to 6·41 in $BaNiO_3$, 5 for all $BaTiO_3$ polymorphs, and 4·62 in $CaTiO_3$. However, the V_A/V_B ratios are experimentally based, and not based on idealized ionic radii, as is the case for the Goldschmidt criterion.

Two further points are raised by application of the polyhedral volume analysis to these compounds. First, Negas' rationalization that variations in temperature and pressure may be 'simulated' by altering the V_A/V_B ratio *chemically* is worthy of further investigation. If this approach is generally valid for oxide ceramics, the polyhedral analysis will be invaluable for understanding the phases obtained at elevated temperatures, for example during sintering or in refractory applications. The prospect then arises for a rational approach to the control of ceramic microstructures, through an adroit choice of impurity ions.

A second point, perhaps of more crystallographic interest, concerns the determination of oxygen-ion positional parameters in these compounds. In much of the literature, idealized oxygen positions have been adopted, since the oxygen-ion X-ray scattering factor is much smaller than those of the cations. However, whenever idealized positions are quoted, the polyhedral analysis cannot be used, since the calculated polyhedral volumes depend solely on the positions of the oxygen ions. Idealized positions will always give a V_A/V_B value equal to 5, although this is unlikely to be correct in systems with *h*-type layers. Thus a case may be made for the re-examination of some of these compounds, for example those with the hexagonal barium titanate structure, by neutron diffraction. Routinely accurate oxygen-ion positional parameters for layered structures would also pave the way for a polyhedral analysis of stacking faults and of polytypism in systems of this kind.

All numerical calculations were carried out on an Apollo DN3000 workstation, using software written by the author. Thanks are due to Mr J. M. Herbert, for bringing the author's attention to these compounds, and for identifying appropriate articles in the literature.

References

BATTLE, P. D., GIBB, T. C. & JONES, C. W. (1988). *J. Solid State Chem.* **74**, 60–66.

BURBANK, R. D. & EVANS, H. T. (1948). *Acta Cryst.* **1**, 330–336.

DICKINSON, J. G., KATZ, L. & WARD, R. (1961). *J. Am. Chem. Soc.* **83**, 3026–3029.

DONOHUE, P. C., KATZ, L. & WARD, R. (1965). *Inorg. Chem.* **4**, 306–310.

DONOHUE, P. C., KATZ, L. & WARD, R. (1966*a*). *Inorg. Chem.* **5**, 335–338.

DONOHUE, P. C., KATZ, L. & WARD, R. (1966*b*). *Inorg. Chem.* **5**, 339–342.

EDWARDS, J. W., SPEISER, R. & JOHNSTON, H. L. (1951). *J. Am. Chem. Soc.* **73**, 2934–2935.

GLAZER, A. M., MABUD, S. A. & CLARKE, R. (1978). *Acta Cryst.* B**34**, 1060–1065.

HARADA, J., PEDERSEN, T. & BARNEA, Z. (1970). *Acta Cryst.* A**26**, 336–344.

JACOBSON, A. J., COLLINS, B. M. & FENDER, B. E. F. (1976). *Acta Cryst.* B**32**, 1083–1087.

JACOBSON, A. J. & HORROX, A. J. W. (1976). *Acta Cryst.* B**32**, 1003–1008.

KATZ, L. & WARD, R. (1964). *Inorg. Chem.* **3**, 205–211.

KOEHL, P. & REINEN, D. (1977). *Z. Anorg. Allg. Chem.* **433**, 81–93.

KRISCHNER, H., TORKAR, K. & KOLBESEN, B. O. (1971). *J. Solid State Chem.* **3**, 349–357.

NEGAS, T. (1973). *J. Solid State Chem.* **6**, 136–150.
NEGAS, T. & ROTH, R. S. (1970). *J. Solid State Chem.* **1**, 409–418.
NEGAS, T. & ROTH, R. S. (1971). *J. Solid State Chem.* **3**, 323–339.
PAULING, L. (1960). *The Nature of the Chemical Bond*, 2nd ed. Ithaca: Cornell Univ. Press.
RANDALL, J. J. & WARD, R. (1959). *J. Am. Chem. Soc.* **81**, 2629–2631.
RAO, C. N. R. & THOMAS, J. M. (1985). *Acc. Chem. Res.* **18**, 113–119.
SASAKU, S., PREWITT, C. T. & BASS, J. D. (1987). *Acta Cryst.* C**43**, 1668–1674.
SCHALLER, H. U. & KEMMLER-SACK, S. (1981). *Z. Anorg. Allg. Chem.* **473**, 178–188.
SCHILDKAMP, W. & FISHER, K. (1981). *Z. Kristallogr.* **155**, 217–226.
SHANNON, R. D. (1976). *Acta Cryst.* A**32**, 751–767.
SHIRANE, G., DANNER, H. & PEPINSKY, R. (1957). *Phys. Rev.* **105**, 856–860.
THOMAS, N. W. (1989). *Acta Cryst.* B**45**, 337–345.
THOMAS, N. W. (1991). *Acta Cryst.* B**47**, 180–191.
THUMM, I., TREIBER, U. & KEMMLER-SACK, S. (1981). *Z. Anorg. Allg. Chem.* **477** 161–166.
TREIBER, U., KEMMLER-SACK, S. & EHMANN, A. (1982). *Z. Anorg. Allg. Chem.* **487**, 189–198.
UPPAL, M. K., RAMASESHA, S. & RAO, C. N. R. (1980). *Acta Cryst.* A**36**, 351–361.

Acta Cryst. (1991). B**47**, 608–617

$BaNiP_2O_7$, a Triclinic Diphosphate with a Modulated Structure of the Displacive Type

BY D. RIOU, H. LELIGNY, C. PHAM,* P. LABBE AND B. RAVEAU

Laboratoire CRISMAT, ISMRa, Bd du Maréchal Juin, 14050 Caen CEDEX, France

(*Received* 19 *November* 1990; *accepted* 1 *March* 1991)

Abstract

The barium nickel diphosphate ($BaNiP_2O_7$) crystals are triclinic [$a = 5{\cdot}317\ (2)$, $b = 7{\cdot}580\ (4)$, $c = 7{\cdot}116\ (2)$ Å, $\alpha = 101{\cdot}26\ (2)$, $\beta = 84{\cdot}48\ (3)$, $\gamma = 89{\cdot}49\ (3)^\circ$] and exhibit an incommensurate modulated structure at room temperature; the modulation is one dimensional and of the displacive type. The wavelength of the modulation wave (13·70 Å) is less than $2b$, where b is the greatest parameter of the basis unit cell; this feature gives rise to a large variation in the atomic configurations throughout the crystal, mainly in the [001] direction [**q*** $-0{\cdot}128\ (2)$, $0{\cdot}047\ (10)$, $0{\cdot}457\ (7)$]. The satellite reflections were collected up to the second order. The modulated structure was solved by a trial and error method and the refinements were performed with the program *REMOS*. The final R values for the main reflections (3866) and the first- and second-order satellite reflections (6922 and 3494) are 0·054, 0·071 and 0·107, respectively. Individually the two PO_4 tetrahedra forming P_2O_7 groups behave as rigid bodies to a good approximation. The more spectacular modulation feature is the very large variation in the Ni—O(6) distances (2·06 to 3·99 Å) through the crystal and correlatively the change of the nickel and barium coordination. As a result the $(NiP_2O_7)_\infty$ chains, running along the a axis, are mixed ribbons involving (Ni_2O_9) and (Ni_2O_8) units. The (Ni_2O_9) units are formed from one NiO_6 octahedron and one NiO_5 pyramid sharing one edge and the (Ni_2O_8) units consist of edge-sharing pyramids. Otherwise, owing to the displacive modulation, regular close connections are found between the $(NiP_2O_7)_\infty$ chains inside the same (010) plane, so leading to a layer structure for $BaNiP_2O_7$. Between these (010) sheets, the cohesion is ensured by interleaved barium cations whose coordination varies from nine to ten.

Introduction

Diphosphates of transition elements with the general formula AMP_2O_7 form a rather limited family of compounds whose mixed framework is generally built up of P_2O_7 groups and MO_6 octahedra. Among them, three diphosphates $CaCoP_2O_7$ (Riou, Labbe & Goreaud, 1988*a*), $BaCoP_2O_7$ (Riou, Labbe & Goreaud, 1988*b*) and $HMn^{III}P_2O_7$ (Durif & Averbuch-Pouchot, 1982) are characterized by a particular association of their polyhedra. Their structures exhibit bioctahedral units of two edge-sharing octahedra linked through tetrahedral diphosphate groups. The recent structural study of $BaCoP_2O_7$ (Riou *et al.*, 1988*b*) allowed the average structure of this triclinic phase to be determined. However some results, particularly the high values of atomic thermal parameters, were found to be not completely satisfactory in view of the quality of the crystals; a disorder phenomenon could not be involved for these crystals since no significant diffuse scattering was observed throughout the reciprocal space. A

* Centre de calcul, Université de Caen.

0108-7681/91/050608-10$03.00